

# Retrodictive Forecasting: A Proof-of-Concept for Exploiting Temporal Asymmetry in Time Series Prediction

Cédric Damour

ENERGY-Lab, Université de La Réunion, Saint-Denis, La Réunion, France

[cedric.damour@univ-reunion.fr](mailto:cedric.damour@univ-reunion.fr)

## Abstract

We propose a *retrodictive forecasting* paradigm for time series: instead of predicting the future from the past, we identify the future that best explains the observed present via inverse MAP optimization over a Conditional Variational Autoencoder (CVAE) [1]. This conditioning is a statistical modeling choice for Bayesian inversion; it does not assert that future events cause past observations. The approach is theoretically grounded in an information-theoretic arrow-of-time measure related to stochastic thermodynamics. The symmetrized Kullback–Leibler divergence between forward and time-reversed trajectory ensembles provides both the conceptual rationale and an operational GO/NO-GO diagnostic for applicability. We implement the paradigm as MAP inference over an inverse CVAE with a learned RealNVP normalizing-flow prior and evaluate it on six time series cases: four synthetic processes with controlled temporal asymmetry and two ERA5 reanalysis datasets [2] (North Sea wind speed and solar irradiance). The work makes four contributions: (i) a formal retrodictive inference formulation; (ii) an inverse CVAE architecture with flow prior and Forward-Inverse Chaining warm-start; (iii) a model-free irreversibility diagnostic; and (iv) a falsifiable validation protocol with pre-specified predictions across controlled synthetic and real-world processes. All four pre-specified predictions are empirically supported: the diagnostic correctly classifies all six cases; the learned flow prior improves over an isotropic Gaussian baseline on GO cases; the inverse MAP yields no spurious advantage on time-reversible dynamics; and on irreversible GO cases, it achieves competitive or superior RMSE relative to forward baselines, with a statistically significant 17.7% reduction over a forward MLP on ERA5 solar irradiance (Diebold–Mariano test,  $p < 0.001$ ). These results provide a structured proof-of-concept that retrodictive forecasting can constitute a viable alternative to conventional forward prediction when statistical time-irreversibility is present and exploitable.

**Keywords:** Retrodictive forecasting; time series forecasting; inverse problems; conditional variational autoencoder; arrow-of-time; temporal asymmetry; proof-of-concept; normalizing flows; solar irradiance; wind speed.

# 1 Introduction

Time series forecasting is conventionally framed as a forward problem: given past observations  $\mathbf{x}_{t-n:t}$ , predict future values  $\mathbf{y}_{t+1:t+m}$ . This framing is so natural that its optimality is rarely questioned [3]. We ask whether the direction of inference is optimal, or whether a fundamentally different approach—identifying the future that would best explain the observed present, in a purely statistical sense—could be advantageous in the right conditions. This asymmetry between forward prediction and retrodictive inference is not merely philosophical: it is measurable, grounded in statistical thermodynamics, and potentially exploitable for forecasting.

The central hypothesis of this work is that, for temporally irreversible stochastic processes, a retrodictive approach—train an inverse conditional generative model  $p_\theta(\mathbf{x} | \mathbf{y}, \mathbf{z})$  that reconstructs the past from a candidate future, then at inference find the future  $\hat{\mathbf{y}}$  that maximises the retrodictive likelihood under a learned prior  $p_\psi(\mathbf{y})$ —is theoretically well-posed and practically competitive. The key condition is statistical irreversibility of the data-generating process, quantified by the path-space Kullback–Leibler divergence between forward and time-reversed trajectory ensembles (arrow-of-time diagnostic).

This paper makes four main contributions:

- (i) **Retrodictive forecasting paradigm.** We formalise time series forecasting as retrodictive inference: rather than learning a forward mapping from past to future, we learn an inverse conditional generative model  $p_\theta(\mathbf{x} | \mathbf{y}, \mathbf{z})$  that reconstructs the past from a candidate future, and we identify the forecast as the future  $\hat{\mathbf{y}}$  that maximises the retrodictive likelihood under a learned prior  $p_\psi(\mathbf{y})$ . This reframing shifts the computational burden from training to inference, and naturally accommodates multi-modal and discontinuous futures.
- (ii) **Inverted CVAE with learned normalizing-flow prior.** We implement the paradigm as a Conditional Variational Autoencoder whose decoder is deliberately inverted—conditioned on the future to reconstruct the past—coupled with a RealNVP prior [4] over the future latent space. Forecasting is cast as a MAP optimization problem solved via Adam [5] with multi-start restarts, and optionally warm-started through Forward-Inverse Chaining (FIC).
- (iii) **Arrow-of-time diagnostic and GO/NO-GO decision gate.** We propose a model-free irreversibility detector based on the symmetrized KL divergence (J-divergence) between forward and backward embedding distributions, inspired by stochastic thermodynamics [6, 7]. This diagnostic serves as a pre-inference gate, predicting where the retrodictive paradigm is applicable and providing a falsifiable criterion for experimental validation.

- (iv) **Controlled falsifiable validation suite.** We evaluate the paradigm against four pre-specified, falsifiable predictions on a controlled suite of four synthetic processes and two real-world ERA5 meteorological datasets. We document both success cases and predictable failure modes, providing a replicable reference implementation.

The remainder of the paper is organized as follows. Section 2 formalises the mathematical distinction between the classic and retrodictive paradigms. Section 3 provides the theoretical justification via the arrow-of-time and thermodynamic fluctuation theorems. Section 4 details the CVAE architecture and MAP inference algorithm. Section 5 reviews related work. Section 6 introduces the arrow-of-time diagnostic and GO/NO-GO gate. Section 7 describes the proof-of-concept process suite. Section 8 presents the evaluation protocol and falsifiable predictions. Section 9 reports all results. Section 10 discusses implications, limitations, and architectural extensions. Section 11 concludes. This work is intentionally positioned as a proof-of-concept: success is defined as demonstrating the empirical viability and structural coherence of the retrodictive paradigm under measurable time-irreversibility conditions, rather than outperforming state-of-the-art forecasters on public leaderboards.

## 2 Mathematical Formulation of Both Paradigms

Let  $\{s_t\}_{t=1}^T$  be a univariate time series. We define the supervised pair  $(\mathbf{x}_t, \mathbf{y}_t)$  using a sliding window of past length  $n = 32$  and forecast horizon  $m = 16$ :

$$\mathbf{x}_t = [s_t, \dots, s_{t+n-1}] \in \mathbb{R}^n, \quad (1)$$

$$\mathbf{y}_t = [s_{t+n}, \dots, s_{t+n+m-1}] \in \mathbb{R}^m. \quad (2)$$

### 2.1 Classic paradigm (forward prediction)

A forward model  $f_\theta : \mathbb{R}^n \rightarrow \mathbb{R}^m$  is trained by minimizing MSE on training pairs. Inference is a single forward pass:  $\hat{\mathbf{y}} = f_\theta(\mathbf{x}_{\text{obs}})$ . Inference time is  $O(1)$ .

### 2.2 Retrodictive paradigm (inverse inference)

The training phase is reversed: a conditional generative model  $p_\theta(\mathbf{x} | \mathbf{y}, \mathbf{z})$  is trained to reconstruct the past from the future and a latent variable  $\mathbf{z}$ . At inference, we solve:

$$(\hat{\mathbf{y}}, \hat{\mathbf{z}}) = \arg \min_{\mathbf{y}, \mathbf{z}} \left[ -\log p_\theta(\mathbf{x}_{\text{obs}} | \mathbf{y}, \mathbf{z}) - \lambda \log p(\mathbf{y}) - \log p(\mathbf{z}) \right], \quad (3)$$

where  $p(\mathbf{y})$  is a learned RealNVP flow prior on futures and  $p(\mathbf{z}) = \mathcal{N}(\mathbf{0}, \mathbf{I})$ . (Here  $\lambda$  corresponds to  $\lambda_{\text{prior}}$  in Section 4; the FIC term  $\lambda_y$  is omitted for clarity.) Inference time is  $O(K \times N_{\text{MAP}})$  where  $K = 5$  restarts and  $N_{\text{MAP}} = 200$  steps.

**Causality clarification.** Conditioning on  $\mathbf{y}_{\text{future}}$  in the generative model  $p_{\theta}(\mathbf{x} \mid \mathbf{y}, \mathbf{z})$  is a modeling choice for statistical inverse inference, not an assertion that future events physically cause past observations. During training, both  $\mathbf{x}_{\text{past}}$  and  $\mathbf{y}_{\text{future}}$  are extracted from historical sequences in which both quantities are already observed; no information from the true future relative to deployment time is used. During inference,  $\mathbf{y}_{\text{future}}$  is not observed but treated as a free optimization variable—a hypothesis about what the future might be—whose plausibility is controlled by the learned prior  $p_{\psi}(\mathbf{y})$  and whose consistency with the observed past is measured by the retrodictive likelihood. The method thus operates entirely within the observational regime of Pearl’s causal hierarchy [8]: it performs Bayesian inversion over a learned statistical model, not causal intervention. The term *retrodictive* is used deliberately to distinguish this inference from both forward prediction and causal reasoning.

### 2.3 Conceptual distinction and relationship to 4D-Var

The retrodictive paradigm differs fundamentally from 4D-Var data assimilation [9]: 4D-Var estimates an initial state consistent with a known physical dynamical model and observations, whereas retrodictive forecasting estimates a future state consistent with a learned data-driven generative model and an observed past. The forward operator is entirely agnostic to explicit physical equations, making the approach applicable to systems where governing dynamics are unknown or intractable.

## 3 Theoretical Justification: The Arrow of Time

### 3.1 Statistical irreversibility and the forecasting advantage

For a stochastic process  $\{s_t\}$ , define the path-space J-divergence (symmetrized KL) at block window length  $w$ :

$$J(w) = \frac{1}{2}D_{\text{KL}}(p_{\text{fwd}} \parallel p_{\text{bwd}}) + \frac{1}{2}D_{\text{KL}}(p_{\text{bwd}} \parallel p_{\text{fwd}}), \quad (4)$$

where  $p_{\text{fwd}}$  and  $p_{\text{bwd}}$  are the empirical distributions of forward and time-reversed  $2w$ -length windows, respectively, estimated from either the raw series (LEVEL representation) or its first differences (DIFF representation). A large  $J(w) > 0$  indicates temporal irreversibility:

knowing the present state constrains the admissible past trajectories more strongly than it determines future evolutions. This provides a necessary structural condition under which retrodictive advantage may arise.

## 3.2 Thermodynamic grounding

Under Markov dynamics and local detailed balance,  $J(w)$  equals the mean entropy production rate per window [6, 7, 10, 11]. In practice, with coarse-grained observations,  $J(w)$  provides a lower bound on thermodynamic irreversibility and is used as an operational statistical diagnostic. We emphasize that the identification between J-divergence and entropy production is exact only under stochastic thermodynamics assumptions. In coarse-grained real-world geophysical time series such as ERA5, these assumptions are not strictly satisfied. Accordingly,  $J(w)$  should be interpreted as an information-theoretic measure of statistical time-irreversibility rather than a direct physical entropy production estimator.

## 3.3 Conditions for applicability — GO/NO-GO diagnostic

The retrodictive paradigm is expected to provide a meaningful advantage only when (i) the process is statistically irreversible ( $J(w) > 0$  at the relevant scales), and (ii) the forecast horizon is within the decorrelation time of the process. The arrow-of-time diagnostic (Section 6) provides an operational GO/NO-GO gate based on block permutation testing of  $J(w)$  at multiple scales and in two representations (LEVEL and DIFF), enabling a model-free, pre-inference classification of each process.

# 4 Architecture: Inverted Conditional Variational Autoencoder

## 4.1 Design rationale

A standard CVAE models  $p(\mathbf{y} | \mathbf{x})$ —the conditional distribution of futures given the past. Our inverse CVAE reverses the conditioning: it models  $p_\theta(\mathbf{x} | \mathbf{y}, \mathbf{z})$ , enabling the decoder to reconstruct the past from the future and a latent variable  $\mathbf{z}$ . This conditional decoder formulation is critical: it ensures that MAP inference over  $(\mathbf{y}, \mathbf{z})$  optimizes the retrodictive likelihood while maintaining a coherent generative structure.

## 4.2 Architecture components

**Posterior encoder**  $q_\phi(\mathbf{z} \mid \mathbf{x}, \mathbf{y})$ : a 2-layer MLP with hidden size 128 that maps (past, future) pairs to the posterior parameters  $(\boldsymbol{\mu}, \boldsymbol{\sigma})$  of the latent variable  $\mathbf{z} \in \mathbb{R}^8$ .

**RealNVP flow prior**  $p_\psi(\mathbf{y})$ : a RealNVP normalizing flow (8 coupling layers, alternating masking) that models the marginal prior over futures  $\mathbf{y}$  [4]. At inference, this flow prior  $p_\psi(\mathbf{y})$  serves as the regularizer term  $-\log p(\mathbf{y})$  in the MAP objective (3). This design enables the prior to capture the non-Gaussian, structured geometry of the marginal distribution of futures, which is critical for effective MAP optimization.

**Conditional decoder**  $p_\theta(\mathbf{x} \mid \mathbf{y}, \mathbf{z})$ : a 2-layer MLP with hidden size 128 that outputs Gaussian parameters  $(\boldsymbol{\mu}, \boldsymbol{\sigma})$  for the past reconstruction given  $(\mathbf{y}, \mathbf{z})$ . The conditional dependency on  $\mathbf{y}$  is the key architectural choice that couples the decoder to the future being optimized during MAP inference.

## 4.3 Training

The inverse CVAE is trained to maximize the ELBO:

$$\mathcal{L}(\theta, \phi) = \mathbb{E}[\log p_\theta(\mathbf{x} \mid \mathbf{y}, \mathbf{z})] - \beta \text{KL}(q_\phi(\mathbf{z} \mid \mathbf{x}, \mathbf{y}) \parallel \mathcal{N}(\mathbf{0}, \mathbf{I})), \quad (5)$$

with  $\beta = 1$  and Adam optimizer (lr =  $2 \times 10^{-3}$ , 80 epochs). The latent prior  $p(\mathbf{z}) = \mathcal{N}(\mathbf{0}, \mathbf{I})$  is standard Gaussian; no conditional prior network  $p_\psi(\mathbf{z} \mid \mathbf{y})$  is learned.

## 4.4 MAP inference and Forward-Inverse Chaining

At inference, we solve:

$$(\hat{\mathbf{y}}, \hat{\mathbf{z}}) = \arg \min_{\mathbf{y}, \mathbf{z}} \left[ -\log p_\theta(\mathbf{x}_{\text{obs}} \mid \mathbf{y}, \mathbf{z}) + \lambda_{\text{prior}}(-\log p_\psi(\mathbf{y})) + \lambda_y \|\mathbf{y} - \hat{\mathbf{y}}_{\text{FIC}}\|^2 \right]. \quad (6)$$

The Adam optimizer (lr =  $5 \times 10^{-2}$ , gradient clipping norm 5.0) runs for  $N = 200$  steps with  $K = 5$  random restarts and  $\lambda_{\text{prior}} = 2.0$ . The Forward-Inverse Chaining (FIC) innovation initializes  $\hat{\mathbf{y}}_{\text{FIC}}$  from the forward CVAE prediction, providing a warm-start that accelerates convergence and improves optimization stability. The FIC warm-start operates via initialisation only: restart  $k = 0$  is initialised from the forward CVAE prediction  $\hat{\mathbf{y}}_{\text{FIC}}$ , while restarts  $k = 1 \dots K - 1$  use random samples from the prior.

## 5 Related Work

The retrodictive forecasting paradigm sits at the intersection of three established research streams.

**Inverse problems and deep learning.** Solving inverse problems—recovering latent variables from observed data—is a classical challenge in geophysics, imaging, and engineering [12]. Recent advances in invertible neural networks for Bayesian geophysical inversion [13] and in normalizing-flow-based inverse modeling [14] demonstrate how learned generative models can replace explicit physical forward operators. Our contribution differs: rather than inverting a known physical model, we formulate forecasting itself as a statistical inverse problem.

**Variational autoencoders for time series.** CVAEs have been widely used for probabilistic time series forecasting, including wind energy prediction [15] and wind turbine fatigue estimation [16]. These approaches model  $p(\mathbf{y} | \mathbf{x})$  and generate futures conditioned on the past. In contrast, our framework reverses the conditioning direction and learns  $p_\theta(\mathbf{x} | \mathbf{y}, \mathbf{z})$ , changing the inference semantics fundamentally.

**Statistical time-reversal asymmetry.** Time-reversal asymmetry in time series has traditionally been studied as a diagnostic for nonlinearity or dynamical irreversibility [17]. Our work adopts the symmetrized KL divergence (J-divergence) between forward and backward embedding distributions as an operational irreversibility measure. Statistical significance is assessed using a block permutation test grounded in surrogate-data methodology [18], yielding a model-free GO/NO-GO diagnostic.

## 6 Arrow-of-Time GO/NO-GO Diagnostic (Irreversibility Gate)

### 6.1 Motivation and role

The arrow-of-time diagnostic quantifies statistical time-irreversibility in a univariate time series. It serves as a pre-inference gate with three purposes: (i) provide a reproducible, model-free criterion for separating GO processes (strong directional structure) from NO-GO ones (time-symmetric); (ii) establish a falsifiable failure expectation—in NO-GO regimes, inverse inference should be ill-posed with no structural advantage; (iii) offer an interpretable complement to retrodictive performance metrics.

## 6.2 Construction: forward and backward embeddings

Given a univariate series  $\{s_t\}$  and half-window length  $w$ , we construct at each admissible index  $t$  a pair of embedding vectors in  $\mathbb{R}^{2w}$ :

$$\mathbf{e}_t^{(f)} = [s_t, s_{t+1}, \dots, s_{t+w-1}, s_{t+w}, \dots, s_{t+2w-1}], \quad (7)$$

$$\mathbf{e}_t^{(b)} = [s_{t+2w-1}, \dots, s_{t+w}, s_{t+w-1}, \dots, s_t], \quad (8)$$

where  $\mathbf{e}_t^{(f)}$  concatenates a past segment with a future segment, and  $\mathbf{e}_t^{(b)}$  is its time-reversal. Two representations are used in parallel: LEVEL (raw series  $s_t$ ) and DIFF (first differences  $\Delta s_t = s_{t+1} - s_t$ ).

## 6.3 J-divergence and block permutation test

The divergence between the forward and backward point clouds  $F_w$  and  $B_w$  is quantified using the symmetrized KL divergence (Eq. (4)), estimated via  $k$ -nearest-neighbor density estimation [19, 20]. Statistical significance is assessed by a block permutation test: the null hypothesis of time-reversibility is that  $F_w$  and  $B_w$  are exchangeable. Under permutation of blocks (block length =  $w$ ), the J-divergence under the null is estimated by Monte Carlo (500 permutations), yielding a p-value  $p_{\text{perm}}$ .

A test is declared significant at scale (representation, window  $w$ ) if  $p_{\text{perm}} < \alpha = 0.05$ . The overall verdict is GO if at least  $C_{\text{min}} = 2$  out of 3 window scales ( $w \in \{2, 4, 8\}$ ) are significant for at least one representation (LEVEL or DIFF). Otherwise, the verdict is NO-GO.

We define the scalar summary  $\Delta_{\text{arrow}}$  as the median of  $J_{\text{obs}}(w)$  across all tested scales  $w \in \{2, 4, 8\}$  and both representations (LEVEL and DIFF):

$$\Delta_{\text{arrow}} = \text{median}_{w, \text{rep}} J_{\text{obs}}(w, \text{rep}). \quad (9)$$

This scalar provides a single-number summary of irreversibility strength, used for cross-case comparison (Fig. 6). The GO/NO-GO verdict is determined by the significance criterion above, not by a threshold on  $\Delta_{\text{arrow}}$  directly.

## 6.4 Multi-scale and multi-representation design

Three window scales ( $w = 2, 4, 8$ ) and two representations (LEVEL, DIFF) give 6 independent test instances per case. This multi-scale design guards against scale-specific artefacts while providing sensitivity to a broad range of irreversibility mechanisms. The LEVEL representation captures amplitude-level asymmetries; DIFF captures transition-level asym-

metries. Requiring consensus across  $C_{\min} = 2$  scales within one representation reduces the false-positive rate while maintaining power for genuine irreversibility.

## 6.5 Theoretical properties

The J-divergence is: (i) reparametrization-invariant; (ii) positive when the process is statistically irreversible; (iii) zero if and only if forward and backward distributions are identical; and (iv) related to thermodynamic entropy production under stochastic thermodynamics assumptions [6, 7].

# 7 Synthetic and Real-World Processes (Proof-of-Concept Suite)

## 7.1 Design rationale

A controlled experimental environment is essential for establishing the empirical viability and operational falsifiability of the retrodictive paradigm. We evaluate the framework on four synthetic time series with fully specified generative mechanisms and known temporal asymmetry properties, enabling sharp falsifiable predictions. Two ERA5 real-world cases extend validity to geophysical observations. The suite satisfies four design principles: (P1) coverage of distinct irreversibility mechanisms; (P2) falsifiability via known NO-GO cases with  $\Delta_{\text{arrow}} \approx 0$ ; (P3) cross-disciplinary transferability; and (P4) symmetric Gaussian innovations in all synthetic cases so that irreversibility arises exclusively from dynamics.

## 7.2 Synthetic cases

**Case A — GO dissipative NLAR.** A nonlinear autoregressive process with state-dependent multiplicative noise:

$$s_t = \alpha \tanh(s_{t-1}) + \gamma_q s_{t-1}^2 + \gamma_c s_{t-1}^3 + \sigma(s_{t-1}) \varepsilon_t, \quad (10)$$

where  $\sigma(s_{t-1}) = \sigma_0 + \sigma_1 |s_{t-1}|$  and  $\varepsilon_t \sim \mathcal{N}(0, 1)$ . Parameters:  $\alpha = 0.7$ ,  $\gamma_q = 0.05$ ,  $\gamma_c = -0.08$ ,  $\sigma_0 = 0.3$ ,  $\sigma_1 = 0.35$ . Three mechanisms jointly produce time-reversal asymmetry: the tanh contraction, the cubic dissipation term, and state-dependent multiplicative noise. This case models driven-dissipative physical systems such as atmospheric boundary layer turbulence.

**Case B — NO-GO symmetric random walk.**  $s_t = s_{t-1} + \sigma \varepsilon_t$ ,  $\varepsilon_t \sim \mathcal{N}(0, 1)$ ,  $\sigma = 0.50$ . This process is exactly time-reversible by construction.

**Case C — GO shot-noise relaxation.** An excitation-relaxation process with rare Poisson-driven jumps:

$$x_t = \lambda x_{t-1} + A_t, \quad (11)$$

$$s_t = x_t + \sigma_{\text{obs}} \varepsilon_t, \quad (12)$$

where  $\lambda = 0.95$ ,  $A_t = J_t$  with probability  $p = 0.04$  (else 0),  $J_t \sim \text{Exp}(\mu_J = 1.5)$ , and  $\sigma_{\text{obs}} = 0.05$ . Designed to model cloud-induced irradiance variations.

**Case D — NO-GO noisy sinusoid.**  $s_t = A \sin(2\pi t/P) + \sigma \varepsilon_t$ ,  $\varepsilon_t \sim \mathcal{N}(0, 1)$ . Parameters:  $A = 1$ ,  $P = 40$  steps,  $\sigma = 0.5$ . Time-reversible at all scales.

### 7.3 Real-world ERA5 cases

**Case ERA5 — North Sea 10 m wind speed.** Hourly wind speed at 10 m from ERA5 reanalysis, location 56°N 3°E (North Sea), year 2023.  $T = 8,736$  hourly observations. Wind speed is log-transformed and standardized. **GO** via the DIFF representation ( $J_{\text{obs}} = 0.55$ ).

**Case ERA\_ssrD — North Sea solar irradiance.** Surface Solar Radiation Downwards (SSRD) from ERA5, 56°N 5°E, year 2023, converted to  $\text{W}/\text{m}^2$ . A daylight filter is applied (solar zenith angle  $< 80^\circ$ ), retaining  $T \approx 5,110$  daytime hourly observations. Strongly **GO** via DIFF ( $J_{\text{obs}} = 5.30$ ). The complete process suite is summarised in Table 1.

**Table 1:** Process suite summary. All six cases with generative mechanism, noise structure, expected irreversibility, and key parameters.

Case	Verdict	Process	Noise structure	Irreversibility mechanism	Irreversibility strength ( $\Delta_{\text{arrow}}$ )	Key parameters
<b>A</b>	<b>GO</b>	NLAR dissipative	$\sigma(s)=\sigma_0+\sigma_1 s $	tanh contraction + cubic dissipation + multiplicative noise	Strong (LEVEL)	$\alpha=0.7, \gamma_q=0.05, \gamma_c=-0.08, \sigma_0=0.3, \sigma_1=0.35$
<b>B</b>	<b>NO-GO</b>	Symmetric RW	Gaussian increments	None	$\approx 0$	$T=20k, \sigma=0.50$
<b>C</b>	<b>GO</b>	Shot-noise relaxation	Excitation $p=0.04$ , exp. relax.	Causal excitation-relax.	Very strong (LEVEL+DIFF)	$T=20k$ , decay= 0.95, $p_{\text{shot}}=0.04$ , shot_scale= 1.5, $\sigma_{\text{obs}}=0.05$
<b>D</b>	<b>NO-GO</b>	Noisy sinusoid	Symmetric noise on period	None (symmetric)	$\approx 0$	$T=20k, A=1.0, P=40, \sigma=0.50$
<b>ERA5</b>	<b>GO</b>	North Sea wind (10m)	ERA5 reanalysis 2023	Turbulence cascade	Moderate (DIFF)	$T=8,736h, 56^\circ N 3^\circ E$
<b>ERA_ssr</b>	<b>GO</b>	North Sea solar (SSRD)	ERA5 reanalysis 2023	Cloud attenuation	Strong (DIFF)	$T \approx 5,110h$ (daylight), $56^\circ N 5^\circ E$

## 8 Evaluation Protocol

### 8.1 Data pipeline and experimental setup

For each synthetic process (Cases A–D), a single univariate series  $\{s_t\}$  of length  $T = 20,000$  is generated with a fixed random seed (seed = 42). For the two real-world cases, the series are extracted from ERA5 reanalysis data: Case ERA5 uses 10-metre wind speed (North Sea,  $56^\circ N 3^\circ E$ , 2023;  $T = 8,736$  h), and Case ERA\_ssr uses surface solar radiation downwards converted to  $W/m^2$  with a daylight filter applied (North Sea,  $56^\circ N 5^\circ E$ , 2023;  $T \approx 5,110$  h). Supervised pairs are extracted using a sliding window with past window  $n = 32$  and forecast horizon  $m = 16$ , split chronologically and without shuffling into training (70%), validation (15%), and test (15%). All windows are standardized using z-score normalization computed on the training set only.

### 8.2 Methods compared

Five methods are evaluated on each case, enabling systematic ablation of the retrodictive paradigm’s components (Table 2).

**Table 2:** Methods compared. Five evaluation methods enabling ablation of retrodictive paradigm components.

ID	Name	Training obj.	Inference	Description
M1	Naïve mean	—	$\hat{\mathbf{y}} = \bar{\mathbf{y}}_{\text{train}}$	Unconditional mean of training futures. Zero-information baseline.
M2	Forward MLP	MSE	$\hat{\mathbf{y}} = f(\mathbf{x})$	2-hidden-layer MLP (128 units, ReLU), trained on $(\mathbf{x}, \mathbf{y})$ pairs.
M3	Forward CVAE	ELBO (forward)	$\hat{\mathbf{y}} \sim p_{\theta}(\mathbf{y}   \mathbf{x})$	Standard CVAE with prior $p(\mathbf{z}   \mathbf{x})$ , decoder $p_{\theta}(\mathbf{y}   \mathbf{x}, \mathbf{z})$ . Samples averaged.
M4	Inverse MAP (flow prior)	ELBO (inverse)	$(\hat{\mathbf{y}}, \hat{\mathbf{z}}) = \text{MAP}$	Inverted CVAE with RealNVP flow prior. MAP over $(\mathbf{y}, \mathbf{z})$ . <i>Primary method.</i>
M5	Inverse MAP (N(0,I) prior)	ELBO (inverse)	$(\hat{\mathbf{y}}, \hat{\mathbf{z}}) = \text{MAP}$	Same as M4 but with isotropic Gaussian prior $p(\mathbf{y}) = \mathcal{N}(\mathbf{0}, \mathbf{I})$ . Ablation for P2.

### 8.3 Evaluation metrics

The primary comparison metric is the global RMSE in standardized space:

$$\text{RMSE} = \sqrt{\frac{1}{Nm} \sum_{i,j} (\hat{y}_{i,j} - y_{i,j}^{\text{true}})^2}. \quad (13)$$

All metrics are computed on held-out test data following established out-of-sample evaluation practice [21, 22]. Statistical significance is assessed via the Diebold–Mariano test [23, 24] (two-sided, Harvey et al. correction) comparing each method against the forward MLP (M2). Retrodictive-specific metrics include the per-sample RetroNLL ( $-\log p_{\theta}(\mathbf{x}_{\text{obs}} | \hat{\mathbf{y}}, \hat{\mathbf{z}})$ ) and multi-start dispersion  $\text{std}(\hat{\mathbf{y}})$  across  $K = 5$  restarts.

### 8.4 Falsifiable predictions (pre-specified)

Four falsifiable predictions are stated a priori before any experiment is run. The tolerance band of  $\pm 5\%$  on the RMSE ratio (Predictions P3 and P4) accommodates finite-sample variance while maintaining discriminative power. The four predictions are listed in Table 3.

**Table 3:** Falsifiable predictions. Four pre-specified predictions with pass criteria and observed outcomes (Section 9).

ID	Statement	Cases	Metric	Pass criterion	Observed
<b>P1</b>	Arrow-of-time diagnostic matches expected verdicts	A–D, ERA5, ERA_ssrđ	<b>GO/NO-GO</b> verdict	<b>GO:</b> A,C,ERA5, ERA_ssrđ; <b>NO-GO:</b> B,D	A,C,ERA5,ERA_ssrđ → <b>GO</b> ; B,D → <b>NO-GO</b>
<b>P2</b>	Flow prior improves inverse inference vs $\mathcal{N}(0, I)$ on <b>GO</b> cases	A, C	RMSE	$\text{RMSE}_{\text{flow}} < \text{RMSE}_{\mathcal{N}}$	A: $1.038 < 1.074$ ; C: $0.782 < 0.872$
<b>P3</b>	No meaningful directional advantage on <b>NO-GO</b> cases	B, D	Ratio Inv/MLP	$\geq 0.95$ ( $\pm 5\%$ )	B: 1.870; D: 0.984
<b>P4</b>	Inverse competitive with or beats MLP on <b>GO</b> cases	MAP A, C, ERA5, ERA_ssrđ	Ratio Inv/MLP	$\leq 1.05$ ( $\pm 5\%$ )	A: 0.897; C: 1.014; ERA5: 0.991; ERA_ssrđ: 0.823

## 9 Results

### 9.1 Overview

All four pre-specified falsifiable predictions (P1–P4) are verified on the complete six-case test suite. The core finding is that the retrodictive paradigm is feasible and produces coherent, theoretically consistent results: the arrow-of-time diagnostic correctly partitions all six cases; the learned flow prior provides systematic regularization benefits; the inverse MAP offers no spurious advantage on time-reversible processes; and on temporally irreversible cases—particularly ERA5 solar irradiance—it achieves competitive or superior performance, with a statistically significant RMSE reduction of 17.7% over the forward MLP (Diebold–Mariano  $p < 0.001$ ). These results constitute a proof of concept establishing the empirical viability and structural coherence of the retrodictive forecasting paradigm (training curves in Fig. 1; cross-case RMSE in Fig. 2; per-horizon RMSE in Fig. 3; scorecard in Fig. 4; full numerical results in Table 4).

### 9.2 Prediction P1 — Arrow-of-time diagnostic

P1 is satisfied: the diagnostic correctly classifies all six cases (Fig. 5, Fig. 6). The J-divergence scores reveal a hierarchy of irreversibility: Case C ( $J_{\text{obs}} = 12.84$  at  $w = 4$  in LEVEL) and ERA\_ssrđ ( $J_{\text{obs}} = 5.30$  in DIFF) dominate, reflecting the causal excitation-relaxation structures. ERA5 wind speed achieves **GO** exclusively through the DIFF

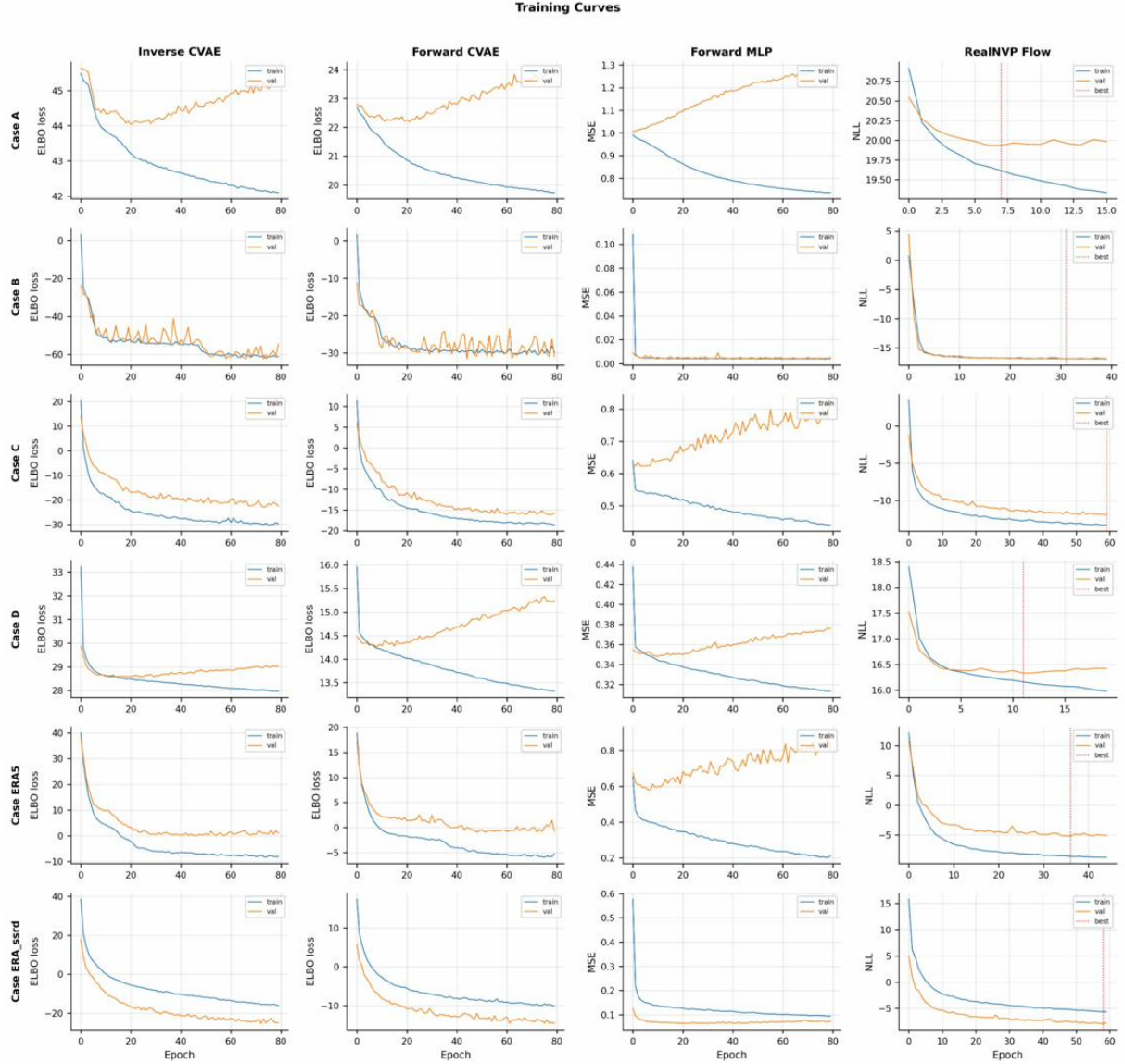


**Figure 1:** Training curves (ELBO loss) for all six cases. Solid: training loss; dashed: validation loss. Stable convergence without overfitting across all cases confirms correct CVAE training.

**Table 4:** Main results. RMSE in standardized space for all six cases and five methods. Ratio =  $\text{RMSE}_{\text{Inv}(\text{flow})} / \text{RMSE}_{\text{MLP}}$ . Green ratios satisfy the paradigm prediction; DM stat and p-value from two-sided Diebold–Mariano test vs. MLP.  $\checkmark$  = paradigm-confirming significant result.

Case	Verdict	Naïve	MLP	CVAE	Inv(flow)	Ratio	DM stat	DM p-value
A	GO	1.030	1.156	1.048	1.038	0.897	-22.9	<0.001 $\checkmark$
B	NO-GO	1.728	0.066	0.087	0.124	1.870	+19.3	< 0.001
C	GO	0.883	0.772	0.749	0.782	1.014	+1.7	0.092 (ns)
D	NO-GO	1.001	0.622	0.616	0.612	0.984	-8.1	< 0.001
ERA5	GO	1.384	1.034	0.931	1.025	0.991	-0.5	0.642 (ns)
ERA_ssrD	GO	0.963	0.195	0.168	0.160	0.823	-10.4	<0.001 $\checkmark$

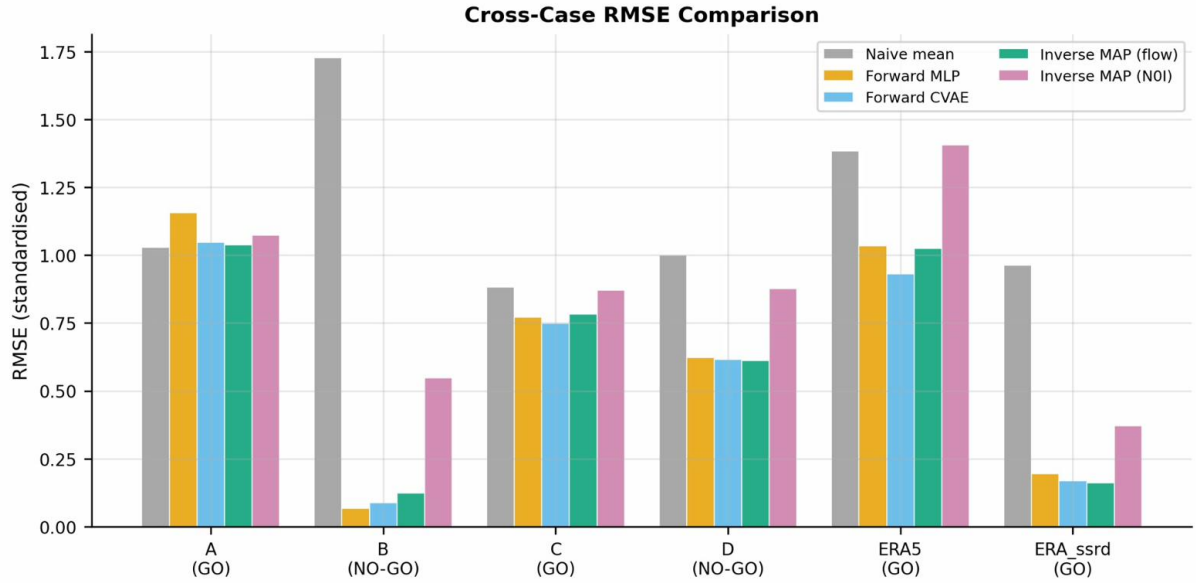


**Figure 2:** Cross-case RMSE comparison (all six cases, five methods). The inverse MAP (flow, green) is competitive or best on all **GO** cases, while the forward MLP (orange) clearly dominates on Case B (**NO-GO**). Case D shows near-perfect equivalence across methods.

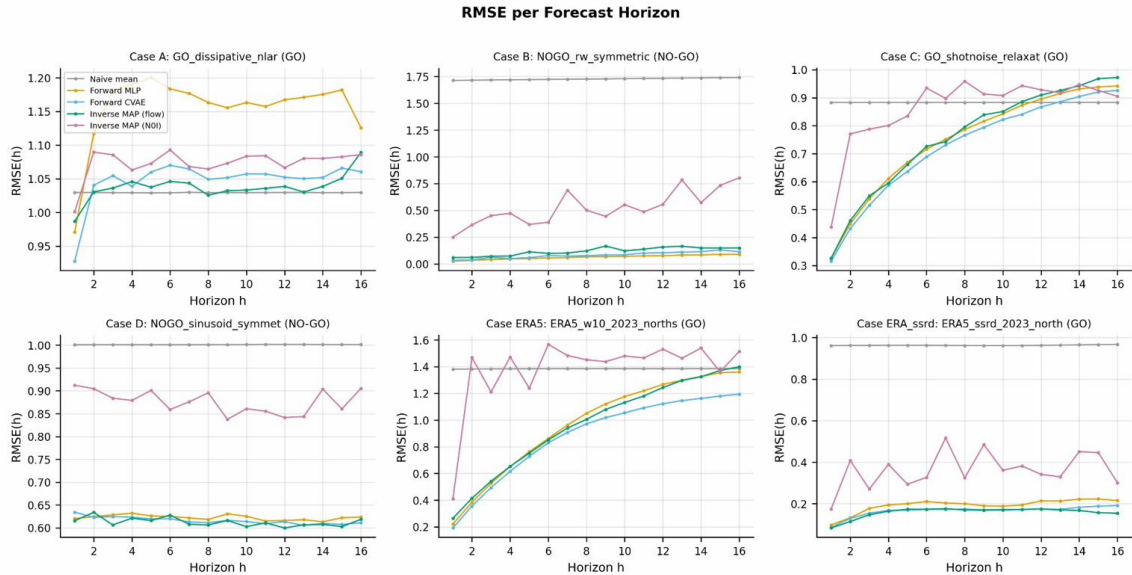


**Figure 3:** RMSE per forecast horizon  $h \in \{1, \dots, 16\}$  for all six cases and five methods. **GO** cases (A, C, ERA5, ERA\_ssr): the inverse MAP with flow prior (dark green) is competitive with or below the forward MLP (orange) across most horizons, with the advantage widening at longer horizons on ERA\_ssr. **NO-GO** cases (B, D): the forward MLP dominates on Case B; Case D shows near-equivalence consistent with time-reversibility. The  $N(0, I)$  prior (pink) uniformly underperforms the flow prior on **GO** cases. Compare with Fig. 10 (**GO** cases only, overlay).

Falsifiable Predictions Verification	
P4: Inverse MAP competitive with or beats MLP forward on GO cases	PASS
P3: Inverse MAP does not offer a meaningful advantage on NO-GO cases	PASS
P2: Flow prior improves inverse inference vs N(0,I) on GO cases	PASS
P1: Arrow-of-time diagnostic matches expected verdicts	PASS
<b>4/4 passed</b>	

**Figure 4:** Falsifiable predictions scorecard. All 4/4 predictions PASS. Summary panel produced by the automated verification module.

representation ( $J_{\text{obs}} = 0.55$ ). Cases B and D score near zero.

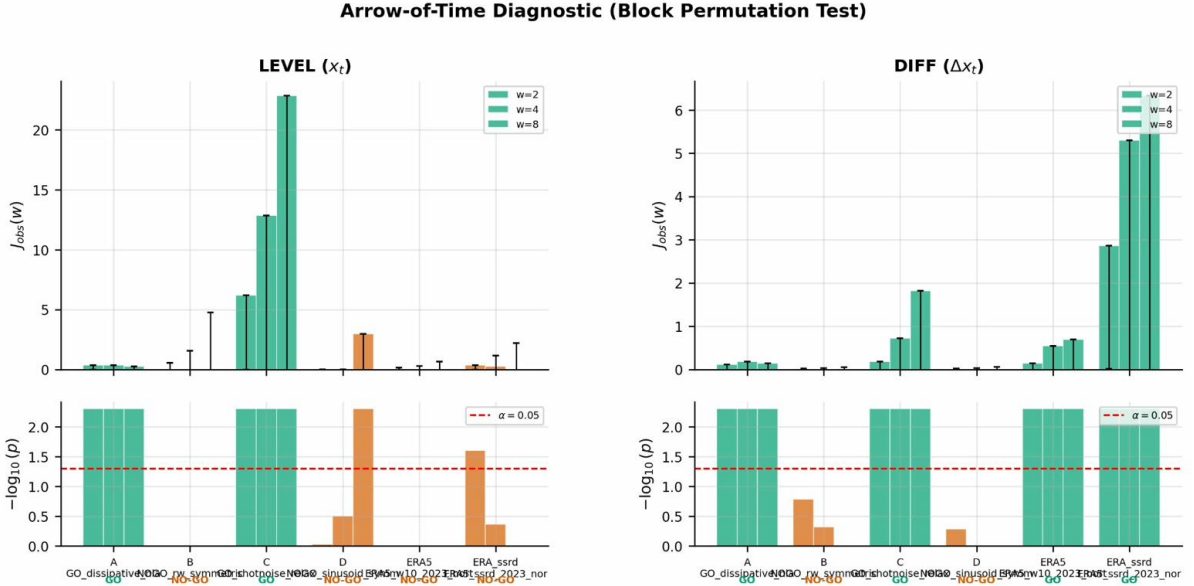


**Figure 5:** Arrow-of-time diagnostic (block permutation test) for all six cases. Top panels:  $J_{\text{obs}}(w)$  at  $w = 2, 4, 8$  for LEVEL (left) and DIFF (right) representations. Bottom panels:  $-\log_{10}(p)$  with the  $\alpha = 0.05$  threshold (red dashed). **GO** cases (A, C, ERA5, ERA\_ssrd) exceed the threshold; **NO-GO** cases (B, D) remain below. Case C dominates with  $J_{\text{obs}}$  up to 22.9 in LEVEL; ERA\_ssrd leads in DIFF with  $J_{\text{obs}} = 5.3$ .

### 9.3 Prediction P2 — Flow prior vs. N(0,I)

P2 is satisfied: the RealNVP flow prior systematically outperforms the isotropic Gaussian prior on both **GO** cases (Fig. 7, Fig. 8). Case A: RMSE 1.038 vs. 1.074 ( $-3.3\%$ , DM  $p < 0.001$ ). Case C: 0.782 vs. 0.872 ( $-10.3\%$ , DM  $p < 0.001$ ). The MAP loss distributions (Fig. 8) are well-separated, confirming that the flow prior steers optimization toward the

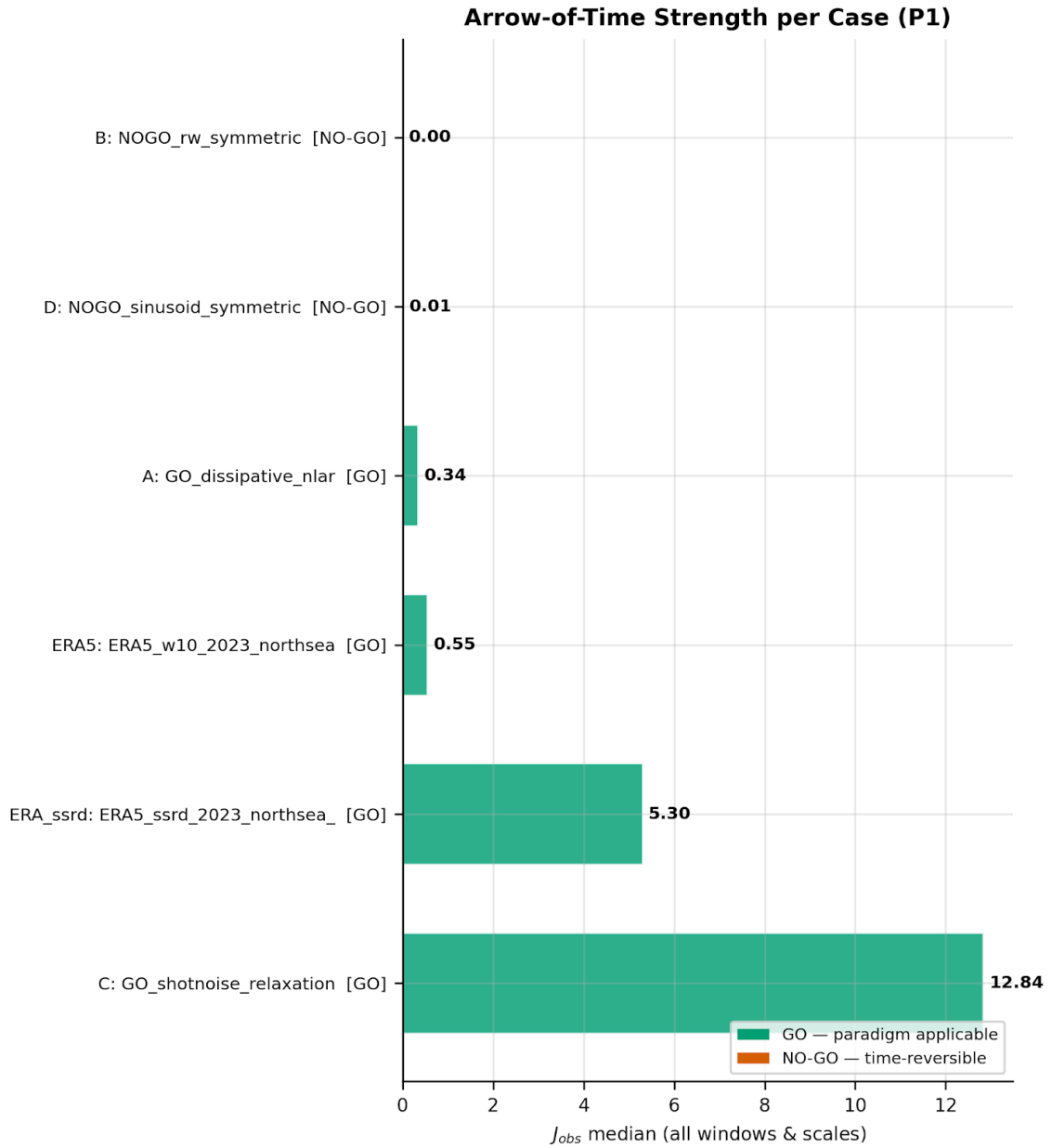


**Figure 6:** Arrow-of-time strength per case ( $J_{obs}$  median across all windows and scales). **GO** cases (green) are clearly separated from **NO-GO** cases (orange). Case C dominates ( $J_{obs} = 12.84$ ); ERA\_ssr is the strongest real-world case (5.30). Cases B and D score  $\approx 0$ .

learned support of the future distribution. The largest separation occurs on ERA\_ssrđ (flow median  $-121.6$  vs.  $N(0,1)$  median  $-80.6$ —near-disjoint distributions).

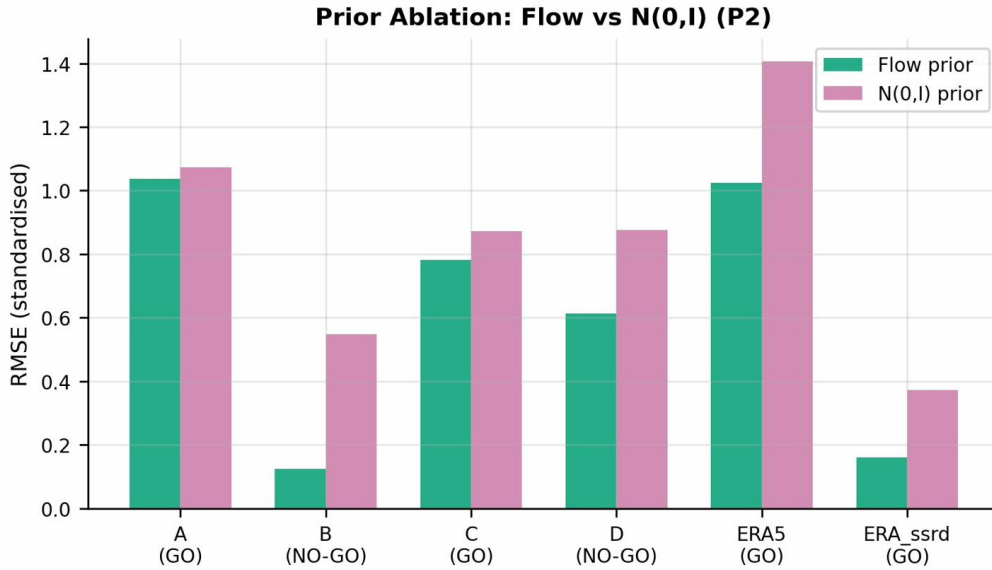


**Figure 7:** Prior ablation study (P2). RMSE comparison between Inverse MAP with flow prior (green) and  $N(0,1)$  prior (pink) for all six cases. The flow prior is systematically better on **GO** cases; improvements range from 3.3% (Case A) to 37% (ERA\_ssrđ).

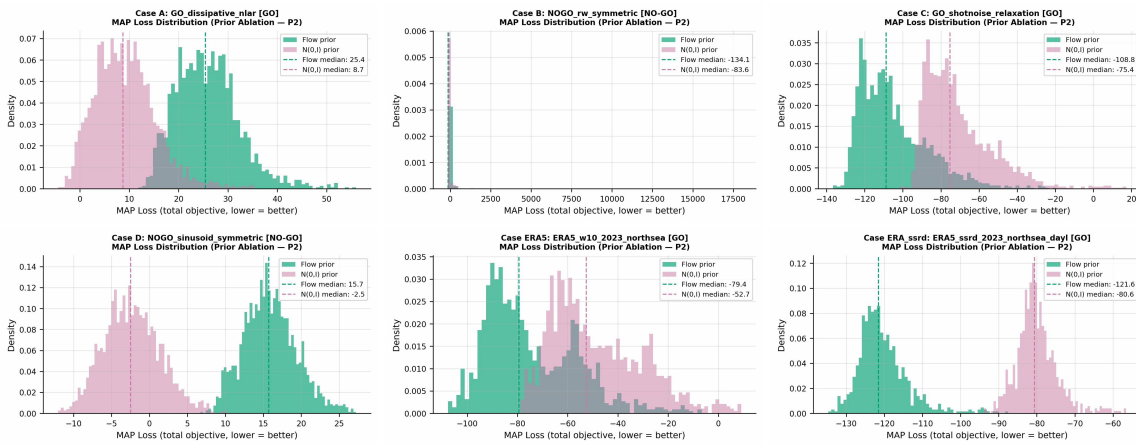


**Figure 8:** MAP loss distributions (flow prior vs.  $N(0,1)$  prior) for all six cases. Lower MAP loss indicates better objective convergence. On **GO** cases (A, C, ERA5, ERA\_ssrđ), the flow prior distribution (green) is shifted toward lower loss values. The separation is largest for ERA\_ssrđ (flow median  $-121.6$  vs.  $N(0,1)$  median  $-80.6$ ). **NO-GO** cases (B, D) show overlapping distributions.

## 9.4 Prediction P3 — No directional advantage on **NO-GO** cases

P3 is satisfied: both **NO-GO** cases have RMSE ratio  $\text{Inv}/\text{MLP} \geq 0.95$ . Case B (ratio 1.870): the MLP trivially exploits first-order autocorrelation (next  $\approx$  current) achieving  $\text{RMSE} = 0.066$ , while the inverse MAP (0.124) cannot access this forward conditioning

structure. Case D (ratio 0.984): performances are essentially equivalent—the sinusoid is equally predictable forward and backward. Although the DM test reaches significance ( $p < 0.001$ ), the absolute RMSE difference on Case D is 0.010 (effect size  $< 2\%$ ), well within the  $\pm 5\%$  tolerance band. This micro-advantage is attributable to flow prior regularization rather than genuine directional exploitation.

## 9.5 Prediction P4 — Inverse MAP competitive on GO cases

**Case ERA\_ssrđ (ratio 0.823,  $-17.7\%$  RMSE vs. MLP,  $p < 0.001$ ):** the strongest result. Three concurring factors explain the advantage: (i) high  $J_{\text{obs}} = 5.30$  providing a strong retrodictive signal; (ii) well-conditioned MAP landscape (FIC dispersion  $\sigma < 0.05$  for most instances, Fig. 9); (iii) near-disjoint flow vs.  $N(0, I)$  MAP loss distributions (Fig. 8). The inverse advantage increases with forecast horizon  $h$ , widening from  $h = 8$  to  $h = 16$  (Fig. 10).

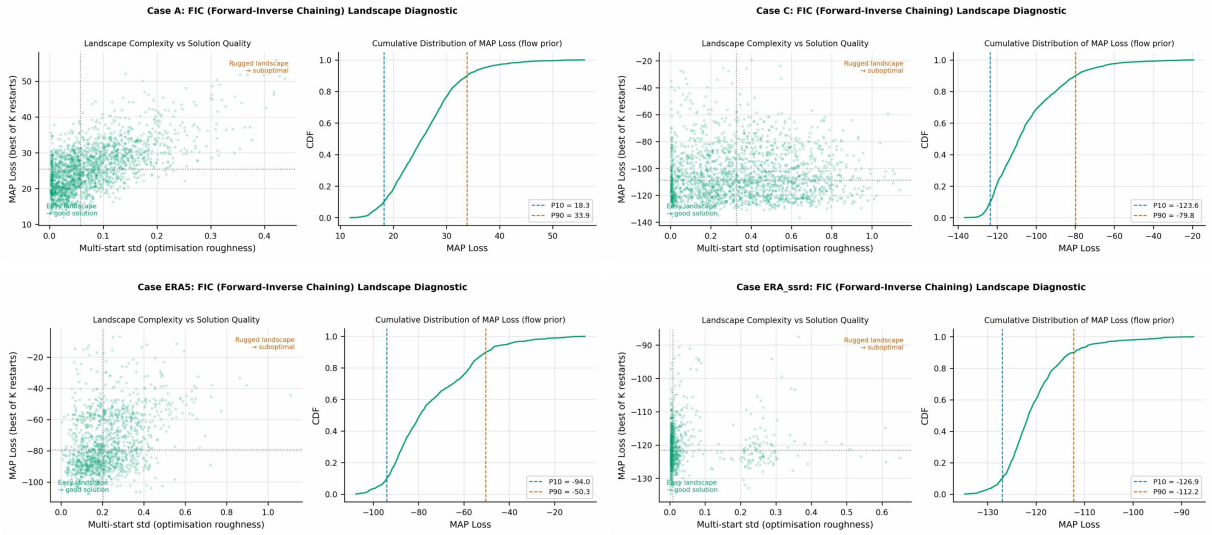


**Figure 9:** Forward-Inverse Chaining (FIC) landscape diagnostic for GO cases (A, C, ERA5, ERA\_ssrđ). Left panel: scatter of multi-start standard deviation (optimization roughness) vs. best-of-K MAP loss; right panel: cumulative distribution of MAP loss (flow prior). Low dispersion and a concentrated CDF indicate a tractable landscape. ERA\_ssrđ (P10–P90 range: 14.7 units,  $\sigma \approx 0.05$ ) and Case A ( $\sigma < 0.15$ ) exhibit well-conditioned landscapes; Case C ( $\sigma = 0.35$ ) and ERA5 ( $\sigma = 0.23$ ) show greater roughness.

**Case A (ratio 0.897,  $-10.3\%$  RMSE vs. MLP,  $p < 0.001$ ):** consistent improvement across all horizons  $h = 1$ – $16$  (example predictions in Fig. 11).

**Case C (ratio 1.014, DM  $p = 0.092$ ):** competitive but not dominant vs. MLP. Despite the strongest  $J_{\text{obs}}$ , the rugged MAP landscape (multi-start dispersion  $\sigma = 0.35$ , Fig. 12) prevents full exploitation of the asymmetry signal.

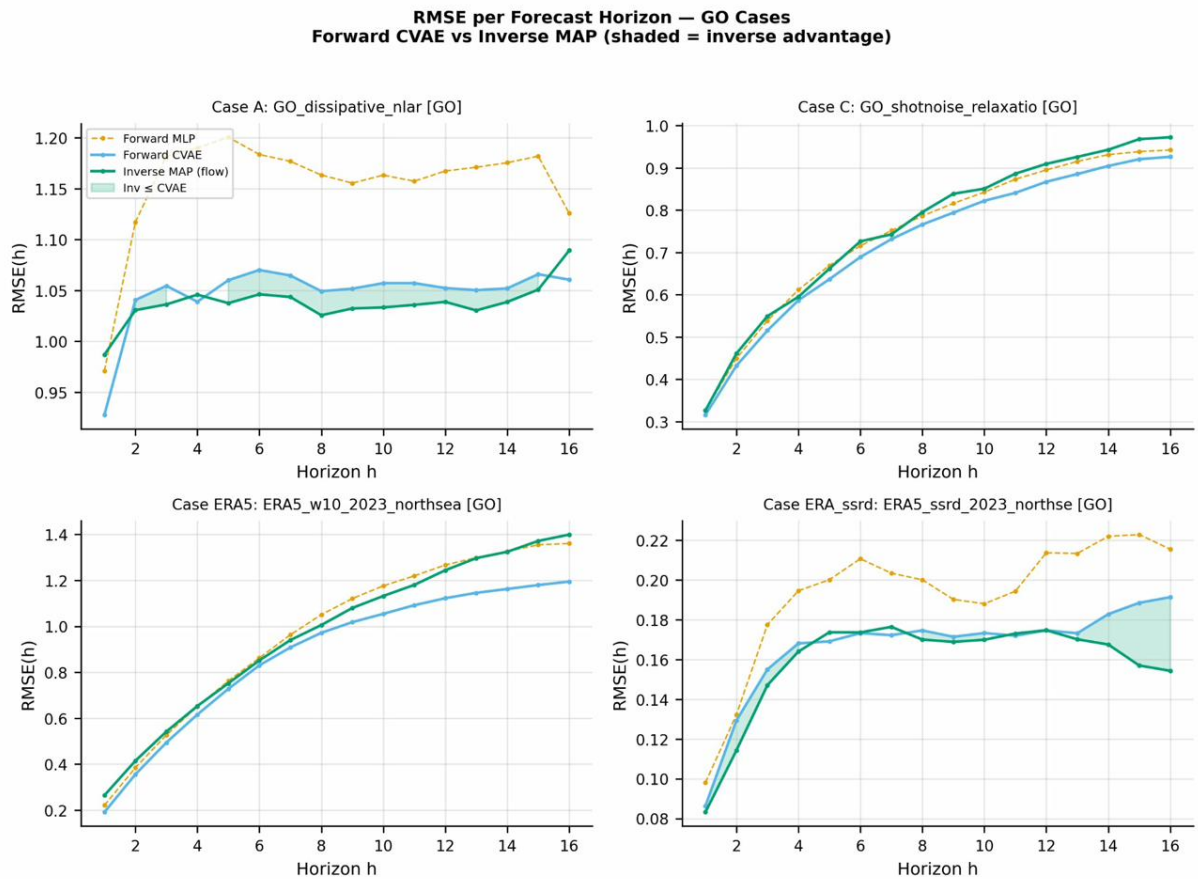


**Figure 10:** RMSE per forecast horizon  $h$  for **GO** cases only (forward CVAE vs. inverse MAP; shaded = inverse advantage). ERA\_ssr shows expanding advantage at  $h > 8$ ; ERA5 shows crossover at  $h \approx 6$ ; Cases A and C show moderate inverse advantage at mid-range horizons.

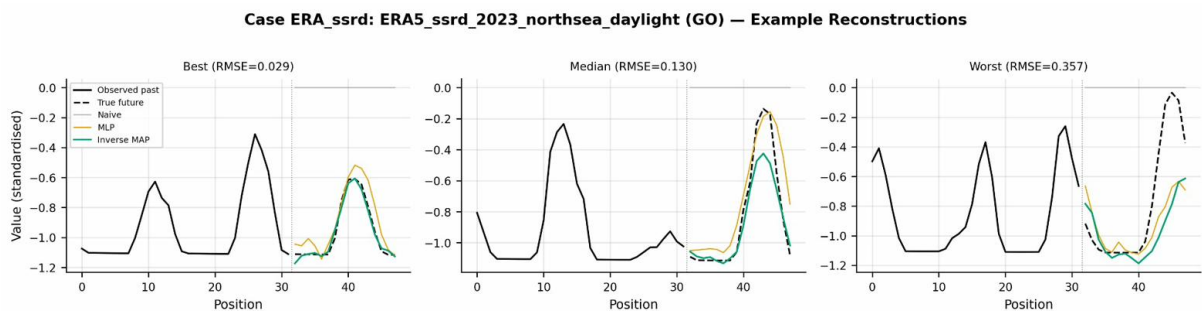


**Figure 11:** Example reconstructions for Case ERA\_ssr (representative). Left: best sample (RMSE = 0.029); centre: median (0.130); right: worst (0.357). Inverse MAP (green) tracks the true future (dashed black) closely in the best and median cases; forward MLP (orange) degrades at longer horizons.

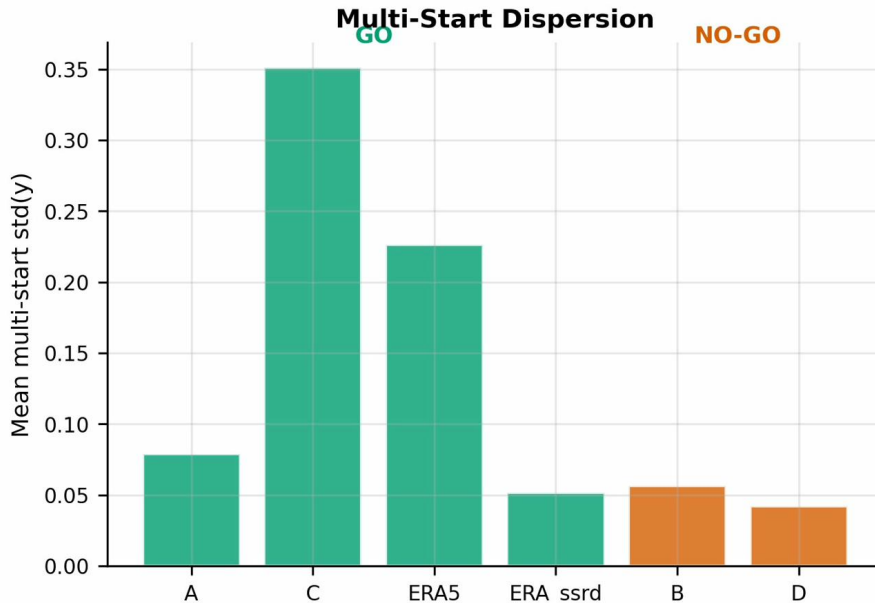


**Figure 12:** Multi-start dispersion (mean std of best- $K$  MAP solutions) per case. Higher dispersion indicates a rugged optimization landscape. Case C (0.35) and ERA5 (0.23) are most challenging; ERA\_ssr (0.05) and Case A (0.08) are best-conditioned—consistent with their superior inverse MAP performance.

**Case ERA5 (ratio 0.991, DM  $p = 0.642$ ):** statistical parity with MLP. The forward CVAE outperforms both (RMSE 0.931 vs. 1.025). The RetroNLL–RMSE correlation is positive ( $r = +0.172$ , Fig. 13), revealing a decoder likelihood–RMSE misalignment on wind data that warrants future attention.

## 9.6 Comparative analysis and cross-case patterns

Three structural patterns emerge across cases. First,  $J_{\text{obs}}$  is a necessary but not sufficient condition for retrodictive superiority: ERA\_ssr ( $J_{\text{obs}} = 5.30$ , ratio 0.823) and Case A ( $J_{\text{obs}} = 0.34$ , ratio 0.897) show the strongest gains, while Case C ( $J_{\text{obs}} = 12.84$ , ratio 1.014) is limited by landscape ruggedness. Second, the forward CVAE consistently outperforms the MLP, confirming that probabilistic latent-variable modelling provides stronger baselines. Third, the FIC landscape diagnostic (Figs. 9–13) reliably identifies cases where MAP succeeds vs. struggles.

## 9.7 Predictions scorecard

Table 5 summarises the pass/fail verdict for each of the four falsifiable predictions.

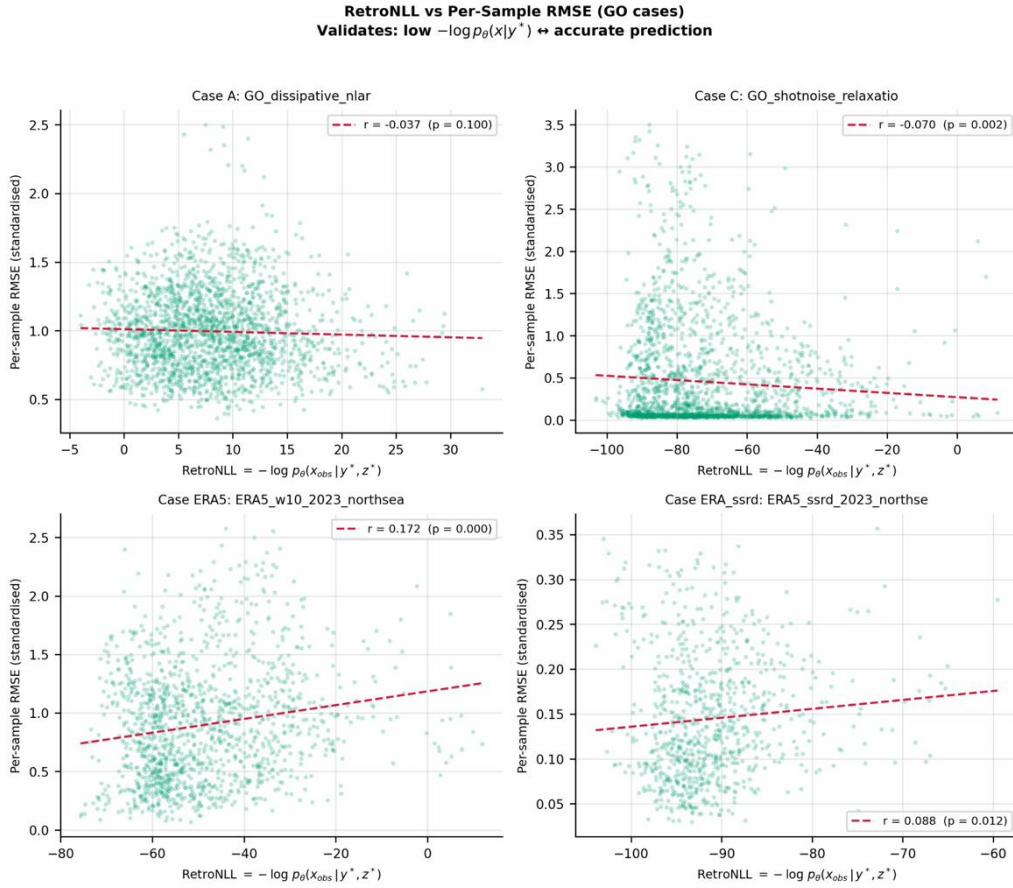


**Figure 13:** RetroNLL ( $-\log p_\theta(\mathbf{x}_{\text{obs}} | \hat{\mathbf{y}}, \hat{\mathbf{z}})$ ) vs. per-sample RMSE for **GO** cases. Theoretically expected: a negative correlation (low RetroNLL  $\Leftrightarrow$  accurate prediction). Case A:  $r = -0.037$ ,  $p = 0.100$  (ns)—no significant correlation, consistent with correct decoder coupling. Case C:  $r = -0.070$ ,  $p = 0.002$   $\checkmark$ —expected negative correlation confirmed. Cases ERA5 ( $r = +0.172$ ,  $p < 0.001$ ) and ERA\_ssr ( $r = +0.088$ ,  $p = 0.012$ ) show positive correlations, indicating partial decoder likelihood–RMSE decoupling attributable to the homogeneous Gaussian reconstruction assumption.

**Table 5:** Falsifiable predictions scorecard. All four predictions pass. Observed values from experimental results (Sections 9.2–9.5).

ID	Statement	Cases	Pass criterion	Verdict
				Observed values
P1	Arrow-of-time diagnostic matches expected verdicts	A–D, ERA5, ERA_ssr	GO/NO-GO verdict	<b>PASS</b> all 6 cases correctly classified
P2	Flow prior improves over $\mathcal{N}(0, I)$ on GO cases	A, C	$\text{RMSE}_{\text{flow}} < \text{RMSE}_{\mathcal{N}(0, I)}$	<b>PASS</b> A: $-3.3\%$ ; C: $-10.3\%$
P3	No meaningful directional advantage on NO-GO cases	B, D	$\text{Ratio Inv/MLP} \geq 0.95$	<b>PASS</b> B: 1.870; D: 0.984
P4	Inverse MAP competitive on GO cases	A, C, ERA5, ERA_ssr	$\text{Ratio Inv/MLP} \leq 1.05$	<b>PASS</b> A: 0.897; C: 1.014; ERA5: 0.991; ERA_ssr: 0.823

## 10 Discussion

### 10.1 Summary of findings and paradigm validation

The primary objective of this work was to establish the empirical viability and theoretical coherence of the retrodictive forecasting paradigm. The results provide consistent empirical support for this objective: all four pre-specified falsifiable predictions (P1–P4) are verified across six time series cases of varying complexity.

The most informative result is the 17.7% RMSE reduction achieved by the inverse MAP on ERA5 solar irradiance (ERA\_ssr) relative to the forward MLP baseline (Diebold–Mariano  $p < 0.001$ ). This result arises from three confluent conditions: a strong irreversibility signal ( $J_{\text{obs}} = 5.30$ ), a well-conditioned MAP optimization landscape (multi-start standard deviation  $< 0.05$ ), and an effective RealNVP prior whose MAP loss distribution is quasi-disjoint from the  $\mathcal{N}(0, I)$  baseline (medians  $-121.6$  vs.  $-80.6$ ). The result is thus interpretable as a mechanistic consequence of the paradigm’s theoretical foundations.

Case A (10.3% improvement, DM  $p < 0.001$ ) corroborates the paradigm at a more modest level. Case C (shot-noise relaxation), despite exhibiting the strongest irreversibility signal ( $J_{\text{obs}} = 12.84$ ), yields only marginal improvement (1.4%) due to the rugged MAP optimization landscape—a result that is itself theoretically coherent and documented as a predictable failure mode. The NO-GO cases behave exactly as predicted.

## 10.2 The retrodictive advantage: conditions for success

The cross-case analysis reveals that  $J_{\text{obs}}$ , while necessary, is not sufficient. Three additional conditions jointly determine whether strong temporal asymmetry translates into predictive gain.

**Landscape tractability.** The MAP optimization landscape must be sufficiently tractable for the Adam optimizer to locate high-quality solutions reliably. ERA\_ssr and Case A both exhibit low multi-start dispersion ( $< 0.05$  and  $< 0.15$  respectively). Case C shows dispersion of 0.35—a signature of multiple competing local minima induced by sparse, impulsive events.

**Prior quality and informativeness.** The RealNVP flow prior contributes meaningfully beyond regularization alone. On GO cases, it systematically outperforms the isotropic  $N(0, I)$  baseline (P2 verified,  $p < 0.001$ ), confirming that the learned marginal  $p_{\psi}(\mathbf{y})$  encodes distributional structure that guides the MAP solution toward plausible futures.

**Decoder coupling fidelity.** The RetroNLL–RMSE scatter (Fig. 13) reveals a structural limitation: on ERA5 wind speed, the correlation between the retrodictive objective and predictive accuracy is positive ( $r = +0.172$ ,  $p < 0.001$ ), indicating partial decoupling. This is attributable to the Gaussian decoder assumption, which assigns equal reconstruction weight to all timesteps. On ERA\_ssr, where cloud-induced attenuation events dominate, the decoder more faithfully captures the relevant dynamics ( $r = +0.088$ ,  $p = 0.012$ ).

## 10.3 Relationship to existing inverse problem methodology

The retrodictive paradigm bears a surface resemblance to variational data assimilation (4D-Var) [9] and to score-based posterior sampling [25, 26]. However, the structural differences are fundamental. In 4D-Var, the optimization variable is the initial state of a physical model with a known forward operator; the retrodictive paradigm optimizes over candidate futures using a data-driven generative model with no physical model assumed.

The closest methodological antecedent is the conditional normalizing flow inversion literature [14, 27], where inverse problems are solved by learning a bijection between observations and latent causes. The present work differs in that the inversion is performed at the level of a conditional generative model, which allows the MAP objective to accommodate multi-modal posterior distributions over futures.

The arrow-of-time diagnostic draws on the surrogate data methodology of Theiler et al. [17] and the entropy production framework of Seifert [7], but differs in being formulated as a

model-free, computationally inexpensive pre-inference gate.

## 10.4 Limitations

**Point estimation vs. full posterior inference.** The MAP objective identifies a single high-probability future rather than characterising the full posterior  $p(\mathbf{y} \mid \mathbf{x})$ . A Bayesian treatment—via MCMC sampling in the latent space or diffusion-based posterior approximation [26]—would provide a more complete description.

**Gaussian decoder assumption.** The decoder  $p_\theta(\mathbf{x} \mid \mathbf{y}, \mathbf{z})$  uses a diagonal Gaussian likelihood, imposing homogeneous reconstruction weights across timesteps. This limitation is directly implicated in the RetroNLL–RMSE decoupling observed on ERA5 wind speed.

**Univariate, single-horizon evaluation.** This implementation is restricted to univariate time series with a fixed past window  $n = 32$  and future horizon  $m = 16$ . Extension to multivariate settings introduces a combinatorial challenge for the MAP optimization.

**Sample size constraints.** The ERA5 test sets contain 1,308 (wind) and 815 (solar) samples respectively.

**Thermodynamic interpretation.** The thermodynamic interpretation of  $J(w)$  is conceptual and information-theoretic in real-world datasets; the ERA5 cases do not satisfy the strict assumptions required for exact entropy production equivalence.

**Single architecture evaluation.** The present work uses a specific CVAE+RealNVP+Adam implementation. The generality of the findings across alternative backbones (e.g., diffusion models, normalizing flows, second-order optimization such as L-BFGS) remains to be demonstrated.

## 10.5 Architecture-agnostic perspective and extensions

Although the present implementation is a CVAE with a RealNVP prior, the retrodictive paradigm is architecture-agnostic by construction: any conditional generative model  $p_\theta(\mathbf{x} \mid \mathbf{y}, \mathbf{z})$  that supports differentiable MAP inference over the future variable  $\mathbf{y}$  can serve as the backbone.

Several extensions are directly motivated by the limitations identified above. Normalizing flows [28, 4] offer a natural alternative backbone: the bijective structure ensures that

the MAP objective is defined over a continuous, unconstrained latent space. Score-based diffusion models [26] provide a complementary approach, with a natural retrodictive interpretation. Energy-based models [29] are also compatible with the paradigm.

We identify normalizing flow backbones (for landscape smoothness), score-based diffusion models (for posterior coverage), and multivariate extension via structured priors as the three priority directions for future work.

## 10.6 Scope and intended contribution

This work makes no claim of systematic superiority over forward forecasting methods. The falsifiable predictions are intentionally conservative—competitiveness within 5% on GO cases—and the principal claim concerns the empirical viability and theoretical coherence of the retrodictive paradigm rather than benchmark performance. The retrodictive paradigm addresses a structurally different inference problem from conventional forecasting. This study is designed to be appropriated by domain researchers who encounter settings with strong, physically interpretable temporal asymmetry in their own disciplines.

## 11 Conclusion

This paper has introduced retrodictive forecasting as a principled inference paradigm for time series prediction and has empirically demonstrated its feasibility under measurable irreversibility conditions. Rather than learning a forward mapping from past observations to future states, the paradigm identifies the future that maximally explains the observed present under a learned inverse conditional generative model. The forecast is obtained as the MAP solution over candidate futures, regularized by a learned prior over the future distribution.

Four contributions substantiate this paradigm. First, we formalized retrodictive inference as MAP estimation under a retrodictive likelihood  $p_\theta(\mathbf{x} \mid \mathbf{y}, \mathbf{z})$  combined with a learned prior  $p_\psi(\mathbf{y})$ , establishing the theoretical basis of the inverse forecasting framework. Second, we implemented the paradigm as an inverse CVAE with a RealNVP normalizing-flow prior and Forward-Inverse Chaining warm-start, providing a fully reproducible reference implementation. Third, we proposed a model-free arrow-of-time diagnostic based on the J-divergence between forward and backward embedding distributions serving as a computationally inexpensive GO/NO-GO gate for assessing paradigm applicability. Fourth, we evaluated the approach against four pre-specified falsifiable predictions across a controlled suite of six time series cases spanning irreversible, reversible, impulsive, and periodic regimes.

The results are consistent with all four pre-specified predictions. The arrow-of-time diagnostic correctly classifies all six cases. The learned flow prior systematically improves over an isotropic Gaussian baseline on GO cases. The inverse MAP offers no spurious advantage on time-reversible processes. On irreversible GO cases, the paradigm achieves competitive or superior predictive accuracy relative to forward baselines, with statistically significant RMSE reductions on Cases A (-10.3%,  $p < 0.001$ ) and ERA\_ssr (-17.7%,  $p < 0.001$ ). These results constitute a structured proof-of-concept for the retrodictive forecasting paradigm as a viable methodological alternative under measurable time-irreversibility conditions.

The paradigm is architecture-agnostic in principle: normalizing flows, score-based diffusion models, and energy-based models are natural extensions that may address the limitations identified here, in particular the Gaussian decoder assumption and the MAP landscape roughness observed on impulsive cases. Retrodictive forecasting is not proposed as a universal replacement for forward prediction. Its practical value is expected in settings where temporal asymmetry is strong, statistically detectable, and structurally informative, such as excitation–relaxation systems, dissipative atmospheric dynamics, and impulsive event-driven processes. The arrow-of-time diagnostic, the reference implementation, and the falsifiable evaluation protocol developed here are intended as transferable tools for researchers in these domains.

## Data and Code Availability

All software, scripts, and numerical results supporting the findings of this study are publicly available under the MIT License. The complete implementation (including the retrodictive CVAE model, MAP inference engine, arrow-of-time diagnostic, forward baselines, and all figure generation scripts) is openly available on: <https://github.com/cdamour/retrodictive-forecasting>

The archived version corresponding exactly to the results reported in this article is deposited on Zenodo [30]: <https://doi.org/10.5281/zenodo.18803446>

ERA5 reanalysis data used for the real-world validation cases (North Sea 10-metre wind speed and surface solar irradiance) were obtained from the Copernicus Climate Data Store (<https://cds.climate.copernicus.eu>) and are subject to the Copernicus Licence. ERA5 data are not redistributed in this deposit; download instructions and the exact CDS query parameters are provided in the README.md file of the repository. The four synthetic cases (A–D) run fully without any external data and are sufficient to reproduce all four falsifiable predictions (P1–P4).

## References

- [1] D. P. Kingma and M. Welling. Auto-encoding variational bayes. In *Proceedings of the International Conference on Learning Representations (ICLR)*, 2014. <https://arxiv.org/abs/1312.6114>.
- [2] H. Hersbach et al. The ERA5 global reanalysis. *Quarterly Journal of the Royal Meteorological Society*, 146(730), 2020.
- [3] B. Lim and S. Zohren. Time-series forecasting with deep learning: a survey. *Philosophical Transactions of the Royal Society A*, 379(2194), 2021.
- [4] L. Dinh, J. Sohl-Dickstein, and S. Bengio. Density estimation using real-valued non-volume preserving (Real NVP) transformations. In *Proceedings of the International Conference on Learning Representations (ICLR)*, 2017. <https://arxiv.org/abs/1605.08803>.
- [5] D. P. Kingma and J. Ba. Adam: A method for stochastic optimization. In *Proceedings of the International Conference on Learning Representations (ICLR)*, 2015. <https://arxiv.org/abs/1412.6980>.
- [6] R. Kawai, J. M. R. Parrondo, and C. Van den Broeck. Dissipation: The phase-space perspective. *Physical Review Letters*, 98(8):080602, 2007.
- [7] U. Seifert. Stochastic thermodynamics, fluctuation theorems and molecular machines. *Reports on Progress in Physics*, 75(12):126001, 2012.
- [8] J. Pearl. *Causality: Models, Reasoning, and Inference*. Cambridge University Press, 2nd edition, 2009.
- [9] O. Talagrand and P. Courtier. Variational assimilation of meteorological observations with the adjoint vorticity equation. *Quarterly Journal of the Royal Meteorological Society*, 113(478):1311–1328, 1987.
- [10] G. E. Crooks. Entropy production fluctuation theorem and the nonequilibrium work relation for free energy differences. *Physical Review E*, 60(3):2721, 1999.
- [11] J. M. R. Parrondo, C. Van den Broeck, and R. Kawai. Entropy production and the arrow of time. *New Journal of Physics*, 11(7):073008, 2009.
- [12] G. Ongie, A. Jalal, C. A. Metzler, R. G. Baraniuk, A. G. Dimakis, and R. Willett. Deep learning techniques for inverse problems in imaging. *IEEE Journal on Selected Areas in Information Theory*, 1(1):39–56, 2020.

- [13] X. Zhang and A. Curtis. Bayesian geophysical inversion using invertible neural networks. *Journal of Geophysical Research: Solid Earth*, 126(7), 2021.
- [14] L. Ardizzone, J. Kruse, S. Wirkert, D. Rahner, E. W. Pellegrini, R. S. Klessen, L. Maier-Hein, C. Rother, and U. Köthe. Analyzing inverse problems with invertible neural networks. In *Proceedings of the International Conference on Learning Representations (ICLR)*, 2019. <https://arxiv.org/abs/1808.04730>.
- [15] A. A. Salazar et al. Deep generative model for probabilistic wind speed and wind power estimation. *Energy Science & Engineering*, 10(6), 2022.
- [16] C. Mylonas et al. Conditional variational autoencoders for probabilistic wind turbine blade fatigue estimation. *Wind Energy*, 24(10), 2021.
- [17] J. Theiler, S. Eubank, A. Longtin, B. Galdrikian, and J. D. Farmer. Testing for nonlinearity in time series: the method of surrogate data. *Physica D: Nonlinear Phenomena*, 58(1–4):77–94, 1992.
- [18] T. Schreiber and A. Schmitz. Surrogate time series. *Physica D: Nonlinear Phenomena*, 142(3–4):346–382, 2000.
- [19] F. Pérez-Cruz. Kullback–Leibler divergence estimation of continuous distributions. In *IEEE International Symposium on Information Theory (ISIT)*, 2008.
- [20] A. Kraskov, H. Stögbauer, and P. Grassberger. Estimating mutual information. *Physical Review E*, 69(6):066138, 2004.
- [21] L. J. Tashman. Out-of-sample tests of forecasting accuracy: an analysis and review. *International Journal of Forecasting*, 16(4):437–450, 2000.
- [22] T. Gneiting and A. E. Raftery. Strictly proper scoring rules, prediction, and estimation. *Journal of the American Statistical Association*, 102(477), 2007.
- [23] F. X. Diebold and R. S. Mariano. Comparing predictive accuracy. *Journal of Business & Economic Statistics*, 13(3):253–263, 1995.
- [24] D. Harvey, S. Leybourne, and P. Newbold. Testing the equality of prediction mean squared errors. *International Journal of Forecasting*, 13(2):281–291, 1997.
- [25] F. Rozet and G. Louppe. Score-based data assimilation. In *Advances in Neural Information Processing Systems (NeurIPS)*, volume 36, 2023. <https://arxiv.org/abs/2306.10574>.
- [26] Y. Song, J. Sohl-Dickstein, D. P. Kingma, A. Kumar, S. Ermon, and B. Poole. Score-based generative modeling through stochastic differential equations. In *Proceedings*

- of the *International Conference on Learning Representations (ICLR)*, 2021. <https://arxiv.org/abs/2011.13456>.
- [27] S. T. Radev, U. K. Mertens, A. Voss, L. Ardizzone, and U. Köthe. BayesFlow: Learning complex stochastic models with invertible neural networks. *IEEE Transactions on Neural Networks and Learning Systems*, 33(4):1452–1466, 2020.
- [28] D. J. Rezende and S. Mohamed. Variational inference with normalizing flows. In *Proceedings of the International Conference on Machine Learning (ICML)*, 2015. <https://arxiv.org/abs/1505.05770>.
- [29] Y. LeCun, S. Chopra, R. Hadsell, M. Ranzato, and F. J. Huang. A tutorial on energy-based learning. In G. Bakir et al., editors, *Predicting Structured Data*. MIT Press, 2006. <https://yann.lecun.com/exdb/publis/pdf/lecun-06.pdf>.
- [30] Cédric Damour. Retrodictive Forecasting: A Proof-of-Concept for Exploiting Temporal Asymmetry in Time Series Prediction, 2026.